Reconfigurable Ferromagnetic Liquid Droplets

Authors:

Xubo Liu[1,2], Noah Kent[2,3], Alejandro Ceballos[6], Robert Streubel[2], Yufeng Jiang[2,5], Yu Chai[2,6,8], Paul Y. Kim[2], Joe Forth[2], Frances Hellman[2,4], Shaowei Shi[1], Dong Wang[1,7], Brett A. Helms[2,8], Paul D. Ashby[2,8], Peter Fischer[2,3], Thomas P. Russell[1,9,10]*

Affiliations:

[1]Beijing Advanced Innovation Center for Soft Matter Science and Engineering, Beijing University of Chemical Technology, Beijing 100029, China

[2]Materials Sciences Division, Lawrence Berkeley National Laboratory, Berkeley, CA 94720, USA

[3]Physics Department, UC Santa Cruz, Santa Cruz CA 95064, USA

[4]Physics Department, University of California, Berkeley, Berkeley, California 94720, USA

[5] Department of Applied Science and Technology, University of California, Berkeley 94720 USA

[6] Department of Materials Science and Engineering, University of California, Berkeley, Berkeley, California 94720, USA

[7]State Key Laboratory of Organic−Inorganic Composites, Beijing University of Chemical Technology, Beijing 100029, China

[8]The Molecular Foundry, Lawrence Berkeley National Laboratory, Berkeley, CA 94720, USA

[9]Polymer Science and Engineering Department, University of Massachusetts, Amherst, MA 01003, USA

[10]WPI–Advanced Institute for Materials Research (WPI-AIMR), Tohoku University, 2-1-1 Katahira, Aoba, Sendai 980-8577, Japan

*Corresponding author: tom.p.russell@gmail.com

Abstract:

Solid ferromagnetic materials are rigid in shape and cannot be reconfigured. Ferrofluids, while reconfigurable, are paramagnetic at room temperature and lose their magnetization when the applied magnetic field is removed. Here, we show a reversible paramagnetic to ferromagnetic transformation of ferrofluid droplets by the jamming of a monolayer of magnetic nanoparticles assembled at the water-oil interface. These ferromagnetic liquid droplets exhibit a finite coercivity and remanent magnetization. They can be easily reconfigured into different shapes while preserving the magnetic properties of solid ferromagnets with classic north-south dipole interactions. Their translational and rotational motions can be actuated remotely and precisely by an external magnetic field, inspiring studies on active matter, energy-dissipative assemblies and programmable liquid constructs.

One Sentence Summary:

Interfacially jammed magnetic nanoparticles transform ferrofluids to reconfigurable ferromagnetic liquid droplets.

Main Text:

Ferromagnetic materials are generally solids with a fixed shape. Reconfigurable magnetic materials are known, such as ferrofluids, dispersions of magnetic nanoparticles in carrier fluids, but they are paramagnetic and lose magnetization once the external magnetic field is removed

(1, 2). Ferrofluids exhibit interesting properties and have found use, for example as magnetic seals, but the inability to retain magnetization limits their broader application. The transformation of a ferrofluid into a ferromagnetic material can be realized by lowering temperature or increasing the viscosity, where Brownian motion of the magnetic nanoparticles (MNPs) is suppressed. Here, we show a simple means to affect this transformation by the *in-situ* formation and interfacial jamming of MNP surfactants.

We immersed an aqueous dispersion of carboxylated 22-nm diameter MNPs (Fe_3O_4-CO_2H) in a solution of amine-modified polyhedral oligomeric silsesquioxane (POSS-NH_2) in toluene. The POSS-NH_2, itself a surfactant, assembles at the interface and electrostatically interacts with the MNPs, anchoring a well-defined number of POSS-NH_2 to the MNPs, converting the MNPs into MNP-surfactants. When the droplet shape changes, the interfacial area increases, and additional MNP-surfactants form and assemble at the interface. The droplet proceeds to re-shape itself to minimize the interfacial area and, thereby, the free energy of the system, but the MNP-surfactants are compressed and jam, locking in the deformed shape *(3, 4)* while remaining magnetized even without an external field.

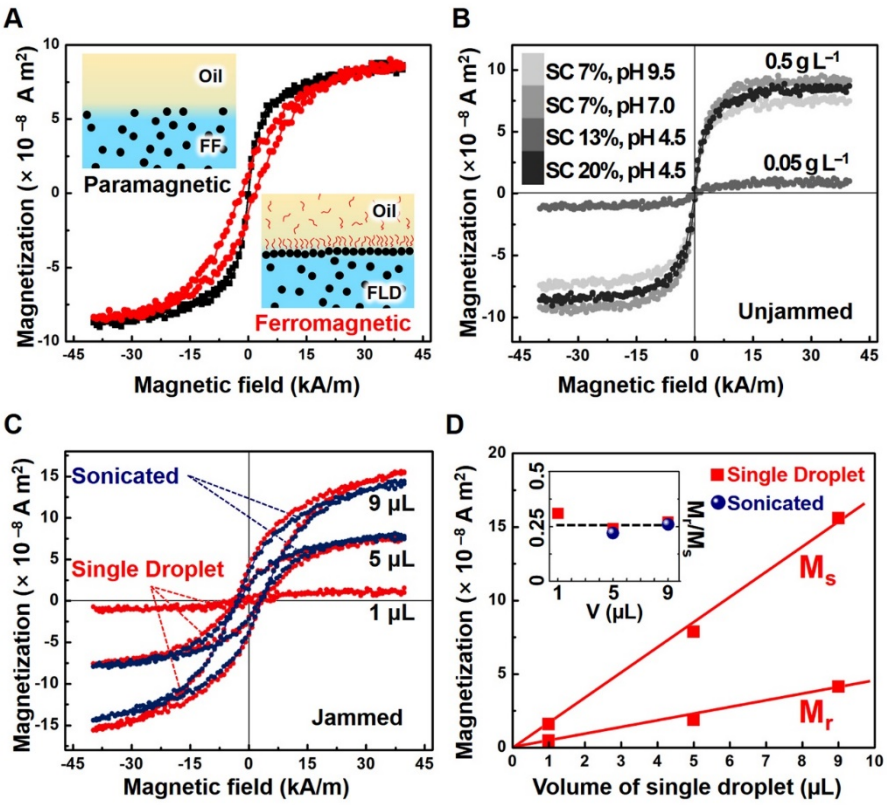

Fig. 1. Tunable transformation of a paramagnetic FF into a FLD by the interfacial jamming of MNPSs. (A) Magnetic hysteresis loops of droplets with (red line) and without (black line) an interfacial layer of jammed MNPSs measured with a vibrating sample magnetometer. Two schematics of aqueous FF and FLD droplet, containing Fe_3O_4-CO_2H MNPs (0.5 g L^{-1}) at pH 4.5, immersed in toluene without and with POSS-NH_2 ligands (1.0 g L^{-1}). **(B)** Hysteresis loops of individual 5 µL aqueous droplets, with 0.5 g L^{-1} and 0.05 g L^{-1} of Fe_3O_4-CO_2H MNPs at different pH, immersed in 0.01 g L^{-1} ligand solution. Surface Coverage (SC) of droplets are ~7 to ~20% where MNPS assemblies are not jammed. **(C)** Hysteresis loops of single, jammed aqueous droplets with 0.5 g L^{-1} of MNPs at pH 4.5 immersed in a 1.0 g L^{-1} solution of POSS-NH_2 in toluene, and hysteresis loops of the same system after being sonicated (Fig. S1 and S2). **(D)** Remanent (M_r) and saturation magnetization (M_s) of the droplets as a function of droplet volume. In the inset, the remanence ratio M_r/M_s as a function of initial droplet volume (single droplet or droplet sonicated into multiple smaller droplets) remains constant at ~0.25.

Magnetic hysteresis loops of Fe_3O_4-CO_2H ferrofluid droplets (Fig. 1A), measured by a vibrating sample magnetometer, show a saturation magnetization (M_s) that depends on the total number of MNPs in the droplets, as well as a vanishing coercive field (H_c) and remanent magnetization (M_r). By adding POSS-NH_2 ligands to the toluene, MNP-surfactants form at the interface. Increasing the concentration of the MNPs in the droplet or decreasing pH, increases the coverage of the interface by MNP-surfactants, reducing the interfacial tension (Fig. S1A, B). With sufficiently surface coverage, the MNP-surfactants jam and the ferrofluid droplet transforms into a ferromagnetic liquid droplet. The magnetic hysteresis loops of identical ferrofluid droplets with and without the jammed interfacial assemblies of MNP-surfactants are shown in Fig. 1A. For both, M_s is the same, since the total number of MNPs is identical, but M_r ~1.89×10^{-8} A m^2 and H_c ~7.2 kA m^{-1} for the ferromagnetic liquid droplet, demonstrating their ferromagnetic character. The jammed, interfacial assemblies of the MNP-surfactants are disordered and have a mechanical rigidity that suppresses thermal fluctuations characteristic of isolated MNPs. The jammed MNPs no longer freely rotate. The spatial separation between adjacent MNP-surfactants is < 5 nm which, combined with the orientation of the dipole magnetization within the MNPs, enhances the thermal stability of the magnetization and transforms the droplet surface into a ferromagnetic layer, similar to a fixed assembly of MNPs *(5, 6)*. When the field is removed, the moment of the ferromagnetic liquid droplet remains until the droplet is exposed to a field exceeding the switching field, whereupon the MNP-surfactant assembly unjams (M_r and H_c vanish), allowing the liquid to be reshaped and re-magnetized. Reshaping the droplet by other external fields or reducing the binding energy of the MNP-surfactants will also unjam the MNP-surfactants, providing further routes to control the magnetization. This ability to manipulate the magnetization further distinguishes ferromagnetic liquid droplets from ferrofluids and common ferromagnetic materials.

If the MNP-surfactant assembly is not jammed, no hysteresis is observed (Fig. 1B). To produce droplets with an unjammed assembly, the surface coverage of the droplets with the MNP-surfactants is varied from 7~20% (Fig. S1C) by changing the concentrations of the MNPs and POSS-NH_2 and the pH. In Fig. 1B variations in M_s arise from differences in the total number of MNPs in each droplet. With full MNP-surfactant coverage, e.g. single droplets of [Fe_3O_4-CO_2H MNPs] = 0.5 g L^{-1} at pH 4.5 in toluene containing [POSS-NH_2] = 1.0 g L^{-1}, the interfacial assembly jams and a typical ferromagnetic hysteresis loop is seen (Fig. 1C). Hysteresis loops were measured for single droplets with different volumes, and the same droplets sonicated into numerous smaller droplets. This preserves the total volume (summed over all droplets) of the MNP dispersions, but increases the surface-to-volume ratio (S/V) by two orders of magnitude (Fig. S2D). M_s and M_r scale linearly with the total volume (total number of MNPs), while H_c remains constant (Fig. 1C). Quite surprisingly, for a given total volume, M_r is independent of S/V with largely varying droplet sizes. The mean separation distance between the dispersed MNPs is ~350 nm, too large for dipolar coupling. For comparison, 100-nm diameter, 10-nm thick nanodiscs with much larger saturation magnetizations are completely uncorrelated when the separation distance is > 60 nm *(7)*. The MNPs dispersed in the droplet freely diffuse, yet a strong coupling and correlation of the dispersed MNPs to those jammed at the interface is evident, and the liquid droplets behave like solid magnets. Furthermore, the ratio of M_r/M_s for the ferromagnetic liquid droplets is 0.25, independent of droplet volume, which is the same as that for frozen ferrofluids at 4.5 K and fixed assemblies of Fe_3O_4 MNPs *(8-10)*. Consequently, ferromagnetic liquid droplets have a similar energy barrier to overcome during magnetization reversal as their frozen/solid counterparts. Therefore, ferromagnetic liquid droplets have the magnetic properties of a solid.

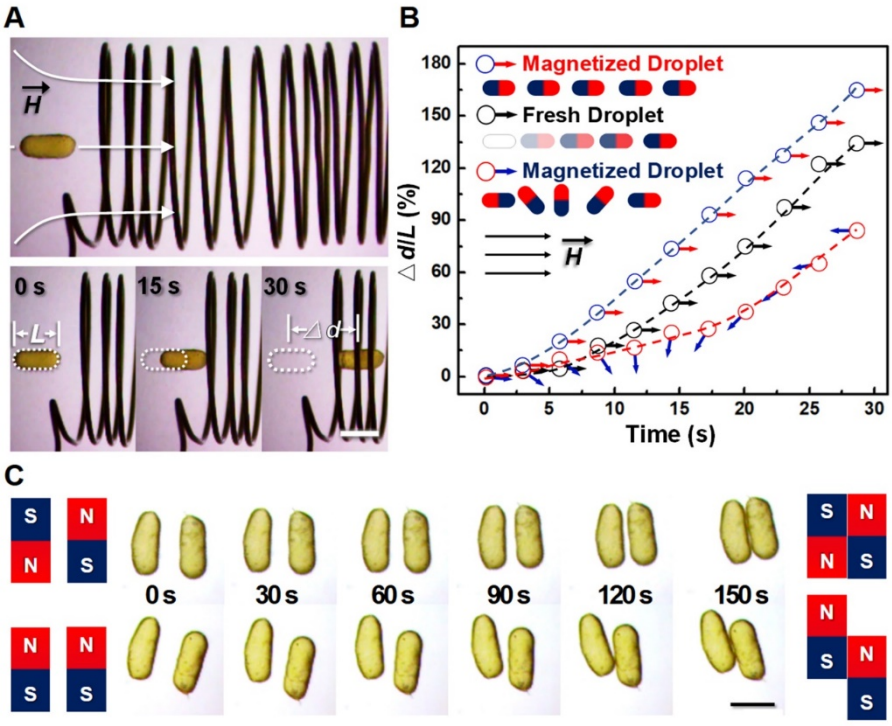

Fig. 2. Manipulating FLDs with magnetic dipole interactions. (A) A magnetized liquid cylinder is attracted by a magnetic field gradient, generated by the aluminum solenoid. **(B)** Displacement as a function of time for fresh non-magnetized liquid cylinder (black arrow), magnetized liquid cylinder with north pole facing the coil (red arrow), and magnetized liquid bar with south pole facing the coil (blue arrow). The ultimate velocity is determined by the field gradient and magnetic moment. The arrows indicate the orientation of the cylinder relative to the initial orientation. **(C)** Dipole interactions, N–S attraction, N–N and S–S repulsion, between two magnetized liquid cylinders. Scale bars, 2 mm.

All-liquid printing *(11-13)* and microfluidics *(14)* were used to produce ferromagnetic liquid cylinders with a 2:1 aspect ratio (Fig. S3). A non-magnetized ferromagnetic liquid cylinder was transferred to a toluene/CCl_4 density gradient where the cylinder descended until buoyant (Fig. S4, A and B). The axis of the cylinder and an insulated solenoid were aligned (Fig. 2A) and a magnetic field of 1~2 kA m^{-1} (Fig. 2B) applied to the solenoid pulled the ferromagnetic liquid cylinder into the solenoid. The cylinder reached the solenoid in 30 s at a speed ~1.1×10^{-4} m s^{-}

[1] and stopped after fully entering the solenoid, due to the absence of drag forces.

The displacement, $\triangle d$, (in units of the droplet length, L) allows comparison of different ferromagnetic liquid cylinders, since the drag force varies linearly with length, which for a fixed cylinder radius, corresponds to the volume and M_s. Figure 2A shows the location and direction of the magnetic moment of the ferromagnetic liquid cylinder. The cylinder magnetized only by the solenoid, moved inside the solenoid (Movie S1). This ferromagnetic liquid cylinder (now magnetized) was re-positioned outside the solenoid, preserving the south-north (S–N) dipole orientation. With the same solenoid magnetic field strength (1~2 kA m^{-1}) the cylinder now accelerates to the solenoid (Fig. 2B, Movie S2). By reversing the field direction of the solenoid (Movie S3), the magnetic moment of the ferromagnetic liquid cylinder and the solenoid field are in antiparallel alignment and should repel each other. However, initially a slight attraction is seen, due to the free MNPs in the cylinder core, then the cylinder rotates, aligning the moment of the jammed MNP-surfactants with the solenoid field, and is drawn into the solenoid (Fig. 2B). Considering the low velocity (v_{max}~1.1×10^{-4} m s^{-1}) and corresponding low Reynolds number (Re ~0.16), the velocity of the ferromagnetic liquid cylinders can be expressed approximately as a function of time: $v(t) = C\frac{ma}{b}\left(1 - e^{-bt/m}\right)$, where C is a dimensionless constant based on Re and the shape of liquid droplet, a is the acceleration from the drag force ($a = F_d / m$), m is the mass, and b is the coefficient of viscous friction. The constant velocity at longer times, independent of the initial magnetization configuration (Fig. 2B), implies a constant solenoid field gradient (due to the same M_s). Deviations from the linear relation in the early stage originate from viscous drag, the varying field gradient outside the solenoid, and the distinct initial magnetization configuration of the cylinder. Consequently, ferromagnetic liquid cylinders behave like solid magnets with N–N, S–S and N–S dipole interactions. Figure 2C shows magnetized liquid cylinders, initially separated by 1 mm, attract each other by such N–S dipole interactions (Movie S4).

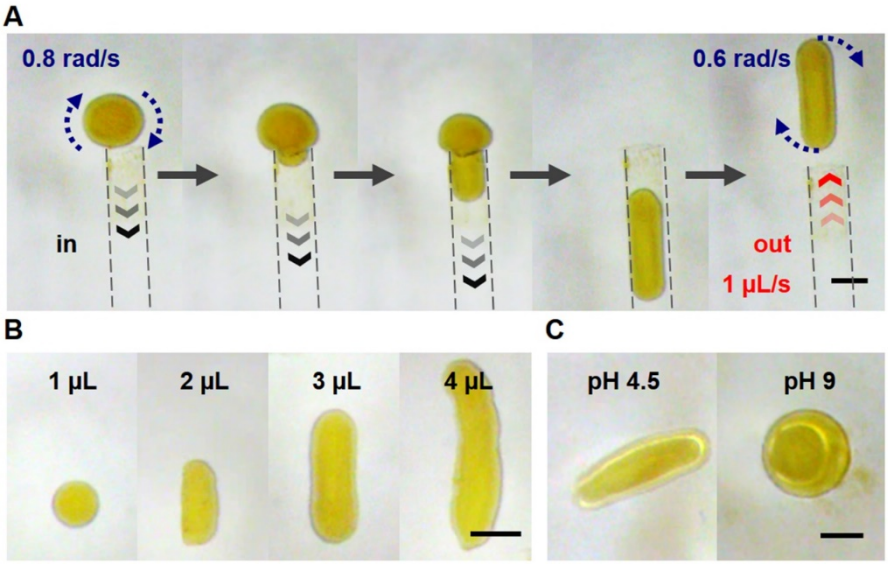

Fig. 3. Top view of deforming a FLD. (A) Reshaping spherical droplet into the cylinder by mechanically molding it with the glass capillary channel. **(B)** Droplets of different aspect ratios can be formed by using droplets with different volumes. **(C)** Reconfiguration of interfacial jamming and unjamming of MNPSs by tuning the pH, e.g., 4.5 and 9 respectively, of aqueous solution in the FLD cylinder. Scale bars, 1 mm.

A distinguishing feature of the ferromagnetic liquid droplets is reconfigurability. A 3-µL spherical ferromagnetic liquid droplet (1.4 mm diameter) was drawn into a 1 mm diameter glass capillary and then rapidly (after several seconds) ejected (Fig. 3A, B, Movie S5). This transformed the spherical droplet into a cylinder (aspect ratio of 3:1). The interfacial area increased by 2.5 times, allowing more MNP-surfactants to form and jam, preserving the cylindrical shape. The ferromagnetic liquid droplet retained its ferromagnetic character, as evidenced by the rotation (~0.6 rad s^{-1}) in response to a rotating permanent magnetic field. The cylinder rotation is slightly less than that of the spherical droplet (~0.8 rad s^{-1}) due to the higher viscous drag force on the cylinder. The shape change can be reversed by tuning the binding energy, as shown in Figure 3C, where the pH was increased from 4.5 to 9, allowing the MNPSs to unjam and the droplet shape reverts to spherical. Magnetization is lost, but by decreasing

the pH, the MNP-surfactants re-jam and the droplet transforms back to a ferromagnetic liquid droplet. So, the shape and magnetic state of the ferromagnetic liquid droplets are responsive.

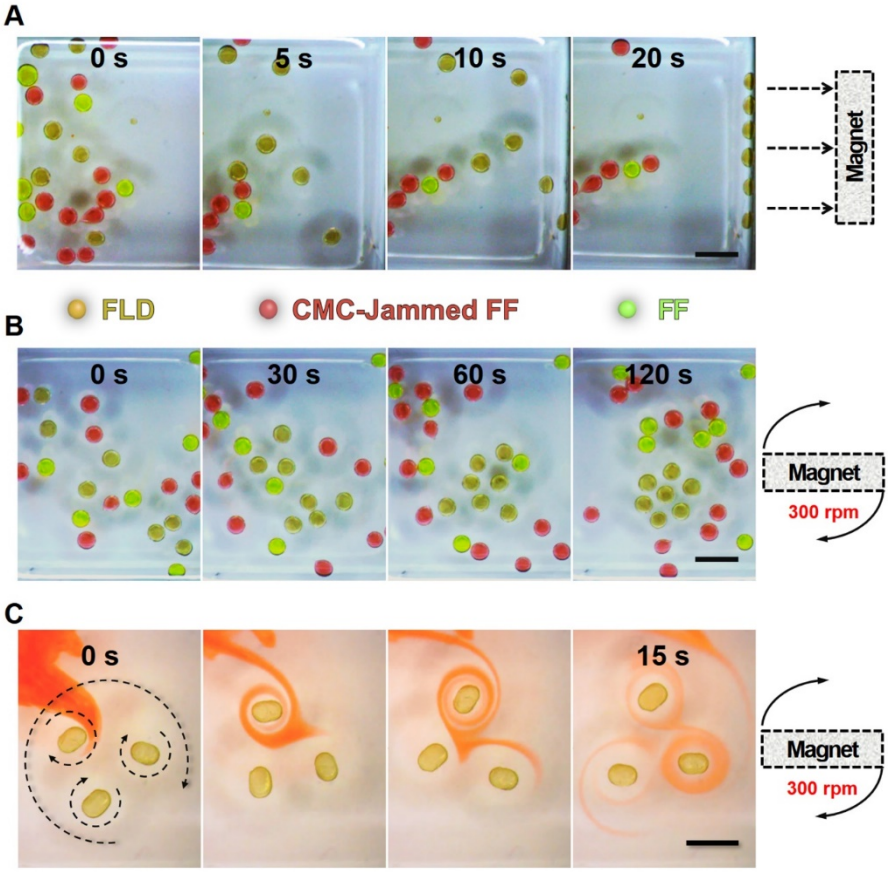

Fig. 4. Sorting FLDs using static and rotational magnetic fields. Mixtures of FLDs comprised of a shell of a jammed monolayer of MNPSs and a FF core (dispersed carboxyl functionalized iron oxide NPs, Fe_3O_4-CO_2H) (brownish spheres), FF droplet comprised of a shell of jammed, non-magnetic carboxymethyl cellulose surfactants (CMCSs) encapsulating an aqueous dispersion of polyethylene glycol coated iron oxide NPs (Fe_3O_4-PEG) (red spheres), FF droplet comprised of an aqueous dispersion of Fe_3O_4-PEG NPs with no jammed monolayer at the droplet surface (bright green spheres). The separation of FLDs using **(A)** a static bar magnet on the side of the container, and **(B)** a bar magnet rotating under the container. [Rhodamine B in CMC jammed FF] = 1 g L^{-1}, [Fluorescein sodium salt in FF] = 1 g L^{-1}. **(C)** Visualization of the hydrodynamic vortex flow for an FLD ensemble rotating magnetic field using an oil soluble dye. [Nile Red in toluene] = 1 g L^{-1}. Scale bars, 3 mm.

The necessity of the magnetic coupling between the interfacially jammed MNP-surfactants and the dispersed MNPs to generate ferromagnetic liquid droplets is shown by changing the nature of the jammed interfacial assembly. Two sets of ferrofluid droplets at a pH of 4.5 were placed in a silicon oil of equal density containing POSS-NH_2 ligands: i) ferrofluid droplets with carboxyl-functionalized 30 nm (22-nm core) Fe_3O_4 MNPs (0.5 g L^{-1}) that form ferromagnetic liquid droplets and ii) a mixture of non-magnetic sodium carboxymethyl cellulose (CMC-CO_2Na) (0.5 g L^{-1}) with 30 nm Fe_3O_4-PEG (non-functionalized) MNPs (0.5 g L^{-1}), where only the CMC interacts with the POSS-NH_2. In both nanoparticles jam at the interface (Fig. 4A) but in the first case they are ferromagnetic, while, in the latter, they are not ferromagnetic. Ferrofluid droplets of only PEG-functionalized Fe_3O_4 MNPs (0.5 g L^{-1}) were also placed in the oil. The total number of MNPs in all the droplets was constant. A bar magnet attracts all droplets (Fig. 4A), since all droplets have a ferromagnetic core, but the ferromagnetic liquid droplets are attracted much more strongly (Fig. 4A, Movie S6). As shown in Fig. 4B, using a rotating magnet, the spherical ferromagnetic liquids rotate, while the unjammed ferrofluid and CMC-jammed ferrofluid droplets do not. The ferromagnetic liquid droplets are also attracted to the center of the magnet and a dynamically stable pattern forms balancing a hydrodynamic repulsion against a magnetic attraction, similar to that observed for elastomer discs *(15, 16)*, or ferrofluids *(17, 18)* containing MNPs. Similar behavior is seen with ferromagnetic liquid cylinders where the vortex flow in the oil is visualized with an oil soluble dye (Fig. 4C, Movie S7). The separation distance between the ferromagnetic liquid droplets depends on the rotation velocity (Fig. S5, Movie S8), as expected. The entire patterned assembly of droplets also rotates in response to the rotating field. Upon stopping the rotating magnet, the ferromagnetic liquid cylinders align along the external field direction (Movie S9). Absent of a dipole moment, the droplets with and without the jammed CMC monolayer do not spin and move only in a

Brownian manner (Movie S10). Therefore, the ferromagnetic liquid droplets can be easily separated, rotated in a controlled manner, and patterned (shown in Fig. 4B), affording a simple strategy for sorting and spatially arranging the ferromagnetic liquid droplets.

In conclusion, we have demonstrated the transformation of a ferrofluid to a ferromagnetic liquid droplet by the interfacial jamming and magnetization of MNPSs. Ferromagnetic liquid droplets have the fluid characteristics of liquids but the magnetic properties of solids. They can be reconfigured while preserving their magnetic properties and the attractive/repulsive interactions between ferromagnetic liquid droplets can be manipulated. Separating and patterning ferromagnetic liquid droplets are easily achieved. The formation of ferromagnetic liquid droplets is reversible, the interfacial assembly of the MNP-surfactants is responsive to external stimuli, and provides systems where translational and rotational motions can be actuated remotely and precisely by an external magnetic field.

References and Notes:

1. S. Odenbach, Ferrofluids and their applications. *MRS Bulletin* **38**, 921-924 (2013).
2. R. E. Rosensweig, Ferrohydrodynamics. (Courier Corporation, 2013).
3. M. M. Cui, T. Emrick, T. P. Russell, Stabilizing Liquid Drops in Nonequilibrium Shapes by the Interfacial Jamming of Nanoparticles. *Science* **342**, 460-463 (2013).
4. Z. Zhang *et al.*, Guiding kinetic trajectories between jammed and unjammed states in 2D colloidal nanocrystal-polymer assemblies with zwitterionic ligands. *Sci Adv* **4**, eaap8045 (2018).
5. A. H. Lu, E. L. Salabas, F. Schuth, Magnetic nanoparticles: synthesis, protection, functionalization, and application. *Angew Chem* **46**, 1222-1244 (2007)
6. J. J. Benkoski *et al.*, Field induced formation of mesoscopic polymer chains from functional ferromagnetic colloids. *J Am Chem Soc* **129**, 6291-6297 (2007)

7. R. Streubel, N. Kent, S. Dhuey, A. Scholl, S. Kevan, P. Fischer, Spatial and Temporal Correlations of XY Macro Spins. *Nano Lett* **18**, 7428-7434 (2018).

8. E. C. S. E. P. Wohlfarth, A mechanism of magnetic hysteresis in heterogeneous alloys. *Philos Trans Roy Soc London. Ser A, Math Phys Sci* **240**, 599-642 (1948).

9. W. Luo, S. R. Nagel, T. F. Rosenbaum, R. E. Rosensweig, Dipole interactions with random anisotropy in a frozen ferrofluid. *Phys Rev Lett* **67**, 2721-2724 (1991).

10. G. F. Goya, T. S. Berquó, F. C. Fonseca, M. P. Morales, Static and dynamic magnetic properties of spherical magnetite nanoparticles. *J Appl Phys* **94**, 3520-3528 (2003).

11. X. Liu, S. Shi, Y. Li, J. Forth, D. Wang, T. P. Russell, Liquid Tubule Formation and Stabilization Using Cellulose Nanocrystal Surfactants. *Angew Chem Int Edit* **56**, 12594-12598 (2017)

12. J. Forth *et al.*, Reconfigurable Printed Liquids. *Adv Mater* **30**, 1707603 (2018).

13. S. Shi, X. Liu, Y. Li, X. Wu, D. Wang, J. Forth, T. P. Russell, Liquid Letters. *Adv Mater* **30**, 1705800 (2018).

14. A. Toor, S. Lamb, B. A. Helms, T. P. Russell, Reconfigurable Microfluidic Droplets Stabilized by Nanoparticle Surfactants. *ACS Nano* **12**, 2365-2372 (2018).

15. L. Derr, A Photographic Study of Mayer's Floating Magnets. *P Am Acad Art Sci* **44**, 525-528 (1909).

16. B. A. Grzybowski, H. A. Stone, G. M. Whitesides, Dynamic self-assembly of magnetized, millimetre-sized objects rotating at a liquid–air interface. *Nature* **405**, 1033 (2000).

17. W. Wang, J. Giltinan, S. Zakharchenko, M. Sitti, Dynamic and programmable self-assembly of micro-rafts at the air-water interface. *Sci Adv* **3**, e1602522 (2017).

18. J. V. I. Timonen, M. Latikka, L. Leibler, R. H. A. Ras, O. Ikkala, Switchable Static and Dynamic Self-Assembly of Magnetic Droplets on Superhydrophobic Surfaces. *Science*

341, 253-257 (2013).

Acknowledgments:

This work was supported by the U.S. Department of Energy, Office of Science, Office of Basic Energy Sciences, Materials Sciences and Engineering Division under Contract No. DE-AC02-05-CH11231 within the Adaptive Interfacial Assemblies Towards Structuring Liquids program (KCTR16). R.S., A.C., N.K., F.H, P.F. acknowledge support from U.S. Department of Energy, Office of Science, Office of Basic Energy Sciences, Materials Sciences and Engineering Division under Contract No. DE-AC02-05-CH11231 within the Non-equilibrium Magnetic Materials program.).Work at the Molecular Foundry (AFM imaging) was supported by the Office of Science, Office of Basic Energy Sciences, of the U.S. Department of Energy under Contract No. DE-AC02-05CH11231. P.D.A. is employed by Scuba Probe Technologies LLC but did not participate in this study in that capacity. S.S. was supported by the Beijing NSF (2194083). X.L. was supported by the Beijing Advanced Innovation Center for Soft Matter Science and Engineering at Beijing University of Chemical Technology, and China Scholarship Council.

Author contributions:

X.L., N.K., R.S., B.A.H., P.D.A., P.F. and T.P.R. made contributions to the conception and design of the experiments. X.L., N.K., A.C., R.S., Y.J., Y.C., J.F., F.H., S.S. and D.W. performed and supported the experiments. X.L., N.K., R.S., P.K., B.A.H., P.D.A., P.F. and T.P.R. interpreted the data and wrote the manuscript.

Competing interests:

The authors declare no competing financial interests.

Data and materials availability:

All data is available in the main text or the supplementary materials

Supplementary Materials:

Materials and Methods

Figures S1-S5

Tables S1

Movies S1-S10

Supplementary Materials for

Reconfigurable Ferromagnetic Liquid Droplets

Xubo Liu, Noah Kent, Alejandro Ceballos, Robert Streubel, Yufeng Jiang, Yu Chai, Paul Y. Kim, Joe Forth, Frances Hellman, Shaowei Shi, Dong Wang, Brett A. Helms, Paul D. Ashby, Peter Fischer, Thomas P. Russell*

Correspondence to: tom.p.russell@gmail.com

This PDF file includes:

Other Supplementary Materials for this manuscript include the following:

Materials and Methods

Chemicals. The following chemicals were used as received from Sigma-Aldrich: Carboxyl-modified iron oxide nanoparticles, (Fe_3O_4-CO_2H NPs, 30 nm). The iron oxide core with 22 nm diameter was coated with a 4 nm thin layer of polymer ligands with carboxyl-end-functionalized, forming a periphery of charged units that stabilizes the NPs dispersion in water; Polyethylene glycol coated iron oxide nanoparticles, (Fe_3O_4-PEG NPs, 30 nm); Amine-modified polyhedral oligomeric silsesquioxane (POSS-NH_2, M_w = 917 g mol^{-1}), Toluene (> 99.8%); Carbon tetrachloride (> 99.9%); Hydrochloric acid (37%); Nile Red (> 98%); Fluorescein sodium salt (acid yellow 73, M_w = 376 g mol^{-1}); Rhodamine B (> 95%); Sodium carboxymethyl cellulose (CMC-CO_2Na, M_w = ~90 Kg mol^{-1}).

Magnetism characterization. A vibrating sample magnetometer (Lakeshore) was used to measure the M-H hysteresis loop of the liquid droplets at room temperature (shown in Fig. S2). For the jamming state of single droplets, the droplet containing a dispersion of MNPs (1, 5 and 9 μL respectively, pH 4.5, [Fe_3O_4-CO_2H MNPs] = 0.5 g L^{-1}) was immersed in ~50 μL of pure toluene ([POSS-NH_2] = 1.0 g L^{-1}) and sealed in a liquid sample holder (730935 Kel-F liquid disposable cup, Lakeshore) for measurements within 2 hr. For the jamming state of emulsified droplets with volume of 5 and 9 μL, the droplet containing MNPs (pH 4.5, [Fe_3O_4-CO_2H MNPs] = 0.5 g L^{-1}) was sealed in the holder and then emulsified by ultrasonication for 10 s. For the unjamming state, pH of the droplets was tuned to 4.5, 7.0, and 9.5 at MNPs concentration of 0.5 g L^{-1}, and pH 4.5 at MNPs concentration of 0.05 g L^{-1}, all of those droplets immersed in the toluene containing 0.01 g L^{-1} of POSS-NH_2, by which the droplet surface cannot reach fully coverage state during the vibrating sample magnetometer measurements.

Measurement of interfacial tensions and surface coverages. An example of the interfacial tension between water and toluene measured with a tensiometer (KRÜSS GmbH, DSA30) is

shown in Fig. S1A, B. The surface coverage $C_s = S_{wrinkling}/S_{free}$ of the MNPs-surfactants at the water/toluene interface was estimated using a pendant drop from the initial volume (surface area, S_{free}) and from the volume of the droplet (surface area, $S_{wrinkling}$) at which the assembly of the MNP-surfactants jammed and began to wrinkle. The droplet is assumed to be rotationally symmetric. The results are shown in Figure S1C. The higher the surface coverage, the less the droplet volume must be reduced before wrinkling is observed.

AFM imaging. An atomic force microscope (AFM, Bruker, Icon) was used to measure the diameter and morphology of MNPs assembled at the water/toluene interface. The assembled film at the water/toluene interface when jamming occurred was retrieved from the liquid interface using a clean silicon wafer and dried at ambient conditions. The AFM image shown in Fig. S4B indicates that the diameter of MNPs at the interface is ~30 nm.

TEM imaging. We transferred a monolayer of jammed NPs to a silicon nitride wafer for TEM imaging. From the TEM image, the particles are ~30 nm. Some particles are quite anisotropic in shape. Depending on the angle between the lattice of the iron oxide atoms and the electron beam, the contrast of the particles will vary. The iron oxide core is also wrapped by a 3~4 nm layer of carboxyl end-functionalized polyetheleneglycol (PEG). The in-surface shape anisotropy leads to disordered packing structure. The nearest-neighbor numbers typically varying from 5 to 8. Images were taken at room temperature using full-field TEM mode with an acceleration voltage of 300 kV (TEAM-1).

Fabrication of liquid cylinders. Using all-liquid 3D printing in a microfluidic device, we continuously printed all-liquid cylinders of the FLD. Upon printing, a slight decrease in the interfacial area jams the MNP-surfactants that form and assemble at the interface. In particular, 2 mm long liquid cylinders with a diameter of 1 mm were printed through a 1 mm diameter PTFE tube, as shown in Fig. S3, by setting a flow rate of the continuous oil phase

containing ligands, Q_O = 30 μL min^{-1}, and that of the aqueous dispersion of Fe_3O_4-CO_2H MNPs, Q_W = 90 μL min^{-1}, respectively. The shape of FLD droplet changes from spherical to cylindrical when $Q_W/Q_O > 1$. If Q_W/Q_O is large enough, a continuous filament of the aqueous phase can be printed in the oil phase.

Fabrication of electromagnetic solenoid. An aluminum wire with ~0.2 mm diameter was wound into a solenoid to generate current-induced magnetic fields that interact with the FLDs. The setup provided a magnetic field of up to 1~2 kA m^{-1} at the center of the solenoid using a current of I = 2 A and N = 15 windings, each separated by L = 1~2 mm. The measured value is in good agreement with the analytical value of H = I/L = 1~2 kA m^{-1}.

Fabrication of density gradient oil phase. The solubility of toluene and CCl_4 in water are 0.051% *w/w* and 0.08% *w/w*, and the dynamic viscosity of toluene and CCl_4 at 20 ˚C are 0.59 cp and 0.97 cp, respectively. They are immiscible with water. Toluene (0.865 g cm^{-3}) is able to segregate and form a thin layer on top of CCl_4 phase (1.595 g cm^{-3}) without fierce shaking, but will form a stable transition layer with a gradient density from 0.865 g cm^{-3} to 1.595 g cm^{-3} at room temperature due to the oil miscibility (see Fig. S4A). This enables the buoyant of water droplets (~1.0 g cm^{-3}) at grade, where volume ratio of toluene to CCl_4 is 4:1 and the dynamic viscosity is ~6.66×10^{-4} kg m^{-1} s^{-1}, while immersing in the oil phase. All the spinning FLDs were imaged in the gradient oil using an optical microscope.

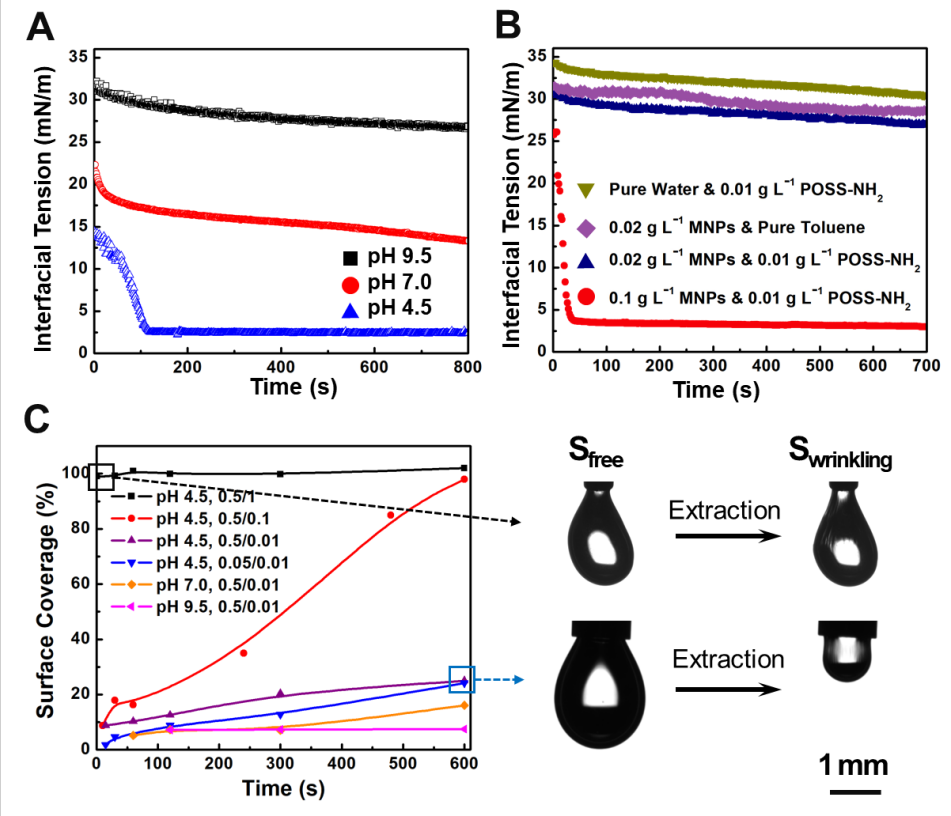

Fig. S1. Temporal evolution of interfacial tension of droplets decorated with MNPs. (A) The influence of pH on interfacial tension is shown for Fe_3O_4-CO_2H MNPs (0.5 g L^{-1}) with POSS-NH_2 (0.01 g L^{-1}). **(B)** Effect of MNPs concentration and respective jamming on interfacial tension for pH 4.5, [POSS-NH_2] = 0.01 g L^{-1}, and [Fe_3O_4-CO_2H MNPs] = 0.02 and 0.1 g L^{-1}. **(C)** Surface coverage of MNPs-surfactants at the water/toluene interface as a function of time for pH 4.5, 7.0, and 9.5, [Fe_3O_4-CO_2H MNPs] = 0.5 or 0.05 g L^{-1}, and [POSS-NH_2] = 0.01, 0.1 or 1 g L^{-1}, respectively. Surface coverage, C_s, is defined as the ratio of surface area at MNPs jamming and free state, respectively, $C_s = S_{wrinkling}/S_{free}$.

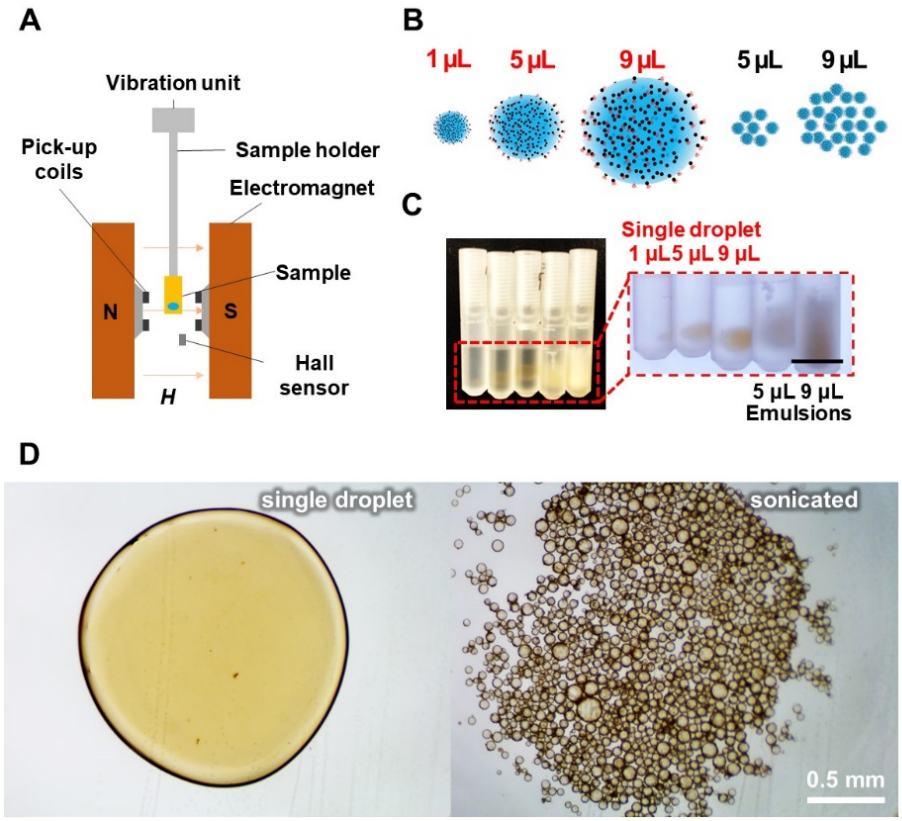

Fig. S2. Vibrating sample magnetometer measurement and liquid sample preparation. **(A)** Schematics of vibrating sample magnetometer for hysteresis loop measurement. **(B)** Schematics and **(C)** images of single droplets with 1 μL, 5 μL, 9 μL and emulsions of sonicated droplets with 5 μL, 9 μL after being ultrasonicated for 10 s, with the surface to volume ratio, *S*/*V*, increasing ~2 orders in magnitude. Scale bars, 5mm. **(D)** 1-μL droplet with a diameter of ~1.5 mm when spread on a glass microscope slide for observation, the mean size of the droplet is ~50 μm after sonication. Scale bar: 0.5 mm.

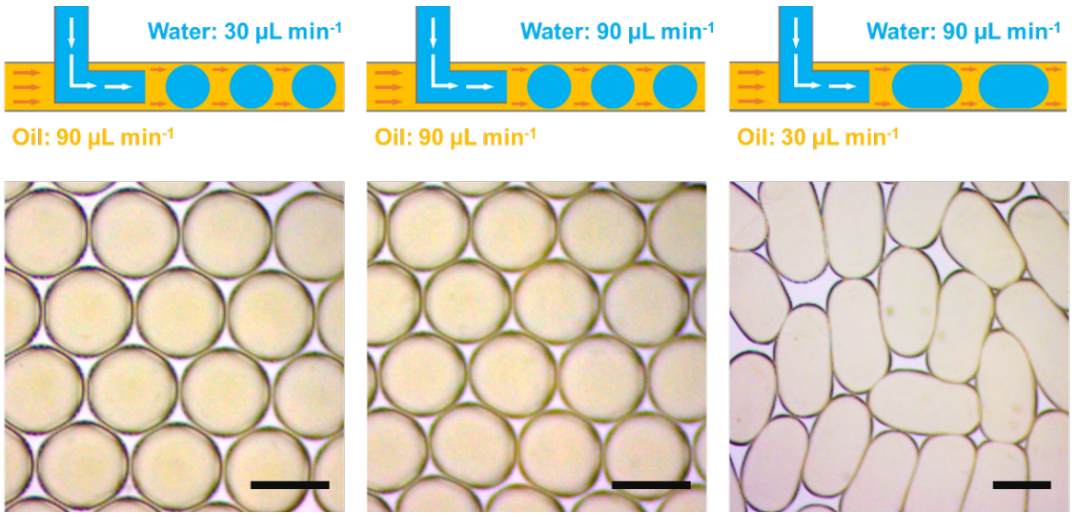

Fig. S3. Shaping droplets by all-liquid 3D printing in microfluidic devices. Shape of the droplets can be optimized by changing diameter and length of PTFE tube, where oil and water mix and flow, and pump-controlled flow rate of water and oil phases. [Fe_3O_4-CO_2H MNPs in water] = 0.5 g L^{-1}, pH 4.5; [POSS-NH_2 in toluene] = 10 g L^{-1}. The printed droplets can be collected using petri dish. Scale bars: 1 mm.

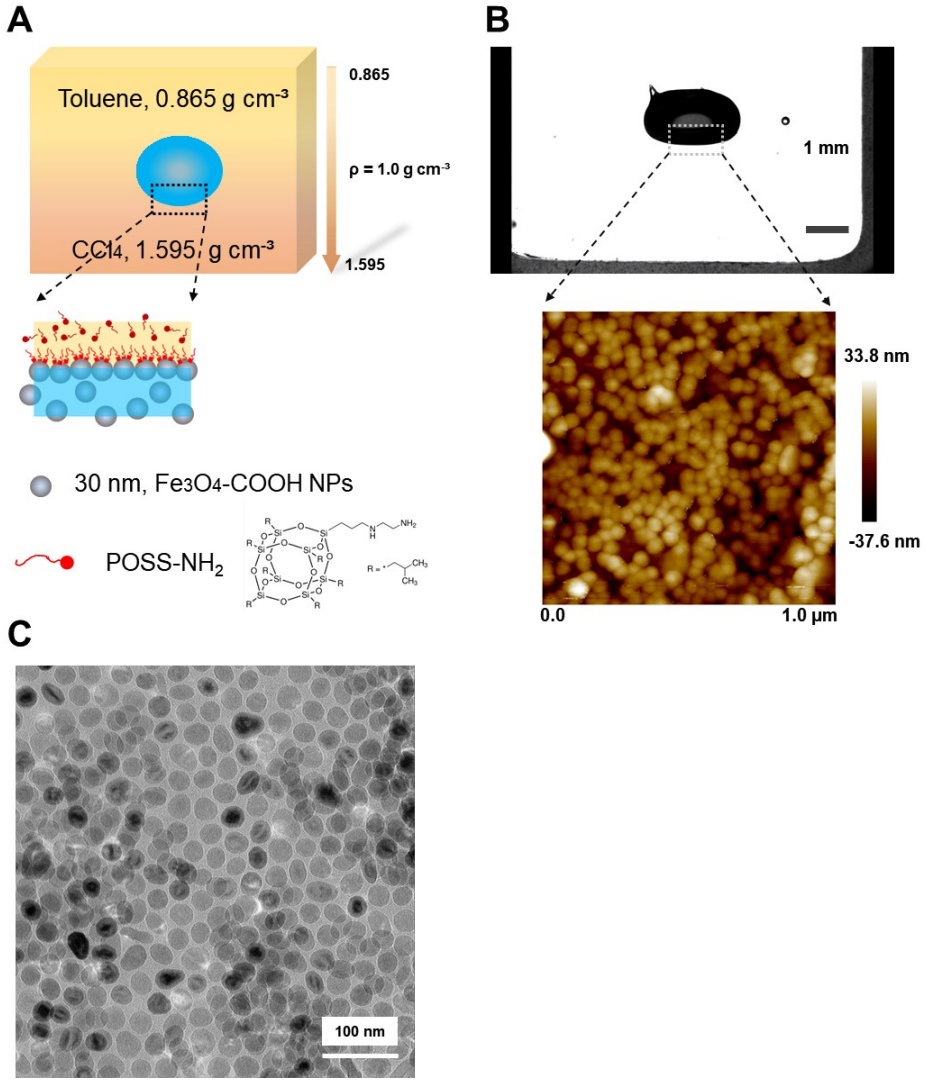

Fig. S4. A droplet buoyant in the gradient oil and morphology of MNPs at interfaces. **(A)** carboxylated iron oxide nanoparticles (Fe_3O_4-CO_2H MNPs) assemble with amine functionalized POSS (POSS-NH_2) at the water/toluene interface. The aqueous droplet (1.0 g cm^{-3}) is buoyant in the bilayer oil mixture of toluene and CCl_4 (v/v=4:1) with a density gradient without any fierce shaking. **(B)** Side-view backlight image of buoyant droplet, stable in the non-spherical shape, indicates that MNPs-surfactants jam at water/oil interfaces very well. The AFM image of the assembled film indicates the jammed state of MNPs at liquid interfaces. The size of nanoparticles is ~30 nm. **(C)** TEM image of jammed MNPs transferred from water-toluene interface to silicon nitride wafer in the dry state.

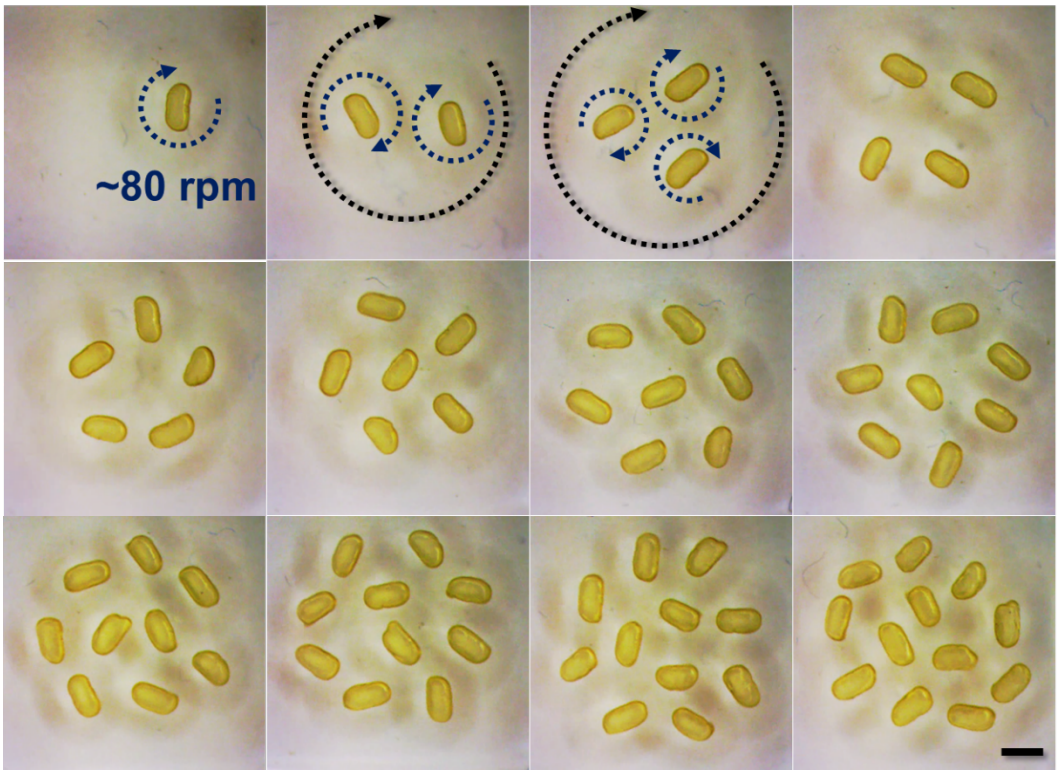

Fig. S5. Top view of stable patterns formed by rotating cylindrical ferromagnetic liquid droplets. Dynamic spinning patterns depend on the droplet numbers (from 1 to 12) and the rotating speed (300 rpm) of the magnet underneath, which generate a rotating magnetic field with a specific strength ($\mu_0 M$ = 1.25 T at surface of the bar magnet). Scale bar: 2 mm.

	Volume (μL)	Saturation Magnetization, M_s ($\times 10^{-8}$ A m^2)	Remanent Magnetization, M_r ($\times 10^{-8}$ A m^2)	Coercivity, H_c (kA m^{-1})	M_r/M_s
Single Droplet	1	1.56	0.48	6.4	0.31
	5	7.86	1.89	7.2	0.24
	9	15.6	4.15	7.2	0.27
Emulsion	5	7.85	1.76	6.0	0.22
	9	14.4	3.70	6.4	0.26

Table S1. Values of saturation magnetization, remanent magnetization, coercive field, and M_r/M_s calculated according to the hysteresis loops.

Movie S1.

A non-magnetized cylindrical ferromagnetic liquid droplet buoyant in the oil is attracted into the solenoid once magnetic field is applied. We observe that the printed FLD cylinder enter into the solenoid with an acceleration after a current is applied to the solenoid to generate a gradient magnetic field. Magnetization happens at first then the attraction makes effect. The video is played with 4 times speed up. The length of the FLD cylinder is 2 mm.

Movie S2.

A magnetized cylindrical ferromagnetic liquid droplet buoyant in the oil is attracted into the solenoid faster. The magnetized FLD cylinder interacts with solenoid by north-south attraction initially, and reaches to the solenoid faster without the magnetization process. The video is played with 4 times speed up. The length of the FLD cylinder is 2 mm.

Movie S3.

A magnetized cylindrical ferromagnetic liquid droplet buoyant in the oil is attracted into the solenoid slower. The repositioned magnetized FLD cylinder rotates to align with the field flux at first due to the south-south repulsion, and then reaches to the solenoid under the north-south attraction. The dipole moment of the FLD cylinder is fixed very well by the interfacial jammed magnetic nanoparticle surfactants. The video is played with 4 times speed up. The length of the FLD cylinder is 2 mm.

Movie S4.

Magnetic N-S dipole interactions between two FLDs. Two magnetized liquid cylinders buoyant in the oil attract each other by coordinated actions of north-south dipole attraction and north-north, south-south repulsions. The video is played at 6 times the actual speed. The volume of the FLD droplets is 2μL and the length of the FLD cylinder is 2 mm.

Movie S5.

Deformation of spherical ferromagnetic liquid droplet into cylindrical shape. A spherical ferromagnetic liquid droplet was drawn into the glass capillary and deformed into a cylindrical shape. The reshaped ferromagnetic liquid droplet was able to rotate, following with the external spinning magnetic field. The video is played at 3 times actual speed. The volume of the ferromagnetic liquid droplet is 2μL and the length of the ferromagnetic liquid cylinder is 2 mm.

Movie S6.

Ferromagnetic liquid droplets are separated from the other paramagnetic liquid droplets by static permanent magnet. The brown spherical FLD droplets with MNPSs jammed at water/oil interfaces move faster after being magnetized than the FF droplets. Separation from the other magnetic droplets is well controlled by external static and rotating magnetic field. The video is played with 2 times speed up. The diameter of droplets is 1 mm.

Movie S7.

A drop of Nile Red toluene solution is added into the gradient oil phase to visualize the flow fields around vortex-generating FLDs. We observe the hydrodynamic radius of a spinning FLD cylinder clearly. The clockwise fluid flow around every FLD s generated vortex-vortex repulsion, leading to the dynamic pattern formation in couple with the magnetic attractions from the rotating magnet. The video is in real time. Scale bar, 2 mm.

Movie S8.

A dynamic pattern is formed by 12 rotating FLD cylinders buoyant in the surrounding oil phase. These patterns are similar with those of Mayer's floating magnets. The attraction to the center of bar magnet and the repulsions between each FLD s result in the special pattern where each FLD stays in the same position relatively. The video is in real time. The length of the FLD cylinder is 2 mm

Movie S9.

Manipulating the orientation of FLD cylinders with an external magnetic field generated by a bar magnet. All magnetized liquid cylinders are aligned along the direction of flow field. They can re-orient immediately along with the changing direction of external magnetic field. The video is in real time. The length of the ferromagnetic liquid cylinder is 2 mm.

Movie S10.

Ferromagnetic liquid droplets are separated from the other paramagnetic liquid droplets by rotating permanent magnet. The spherical FLD droplets with dipole moment rotate along with the rotating magnetic field and form patterns due to the hydrodynamic repulsion and magnetic attraction. The red and fluorescent green paramagnetic droplets without dipole moment only move along with the rotating field randomly, and are expelled from the central area by the vortex flow. The video is played with 6 times speed up. The diameter of droplets is 1 mm.